IEEE Photonics Journal
An IEEE Photonics Society Publication

Open Access

Power-Efficient Kerr Frequency Comb Based Tunable Optical Source

Volume 9, Number 3, June 2017

S. Arafin, *Member, IEEE*
A. Simsek, *Student Member, IEEE*
S.-K. Kim
W. Liang
D. Eliyahu
G. Morrison
M. Mashanovitch, *Senior Member, IEEE*
A. Matsko, *Senior Member, IEEE*
L. Johansson, *Member, IEEE*
L. Maleki, *Fellow, IEEE*
M. J. Rodwell, *Fellow, IEEE*
L. A. Coldren, *Life Fellow, IEEE*

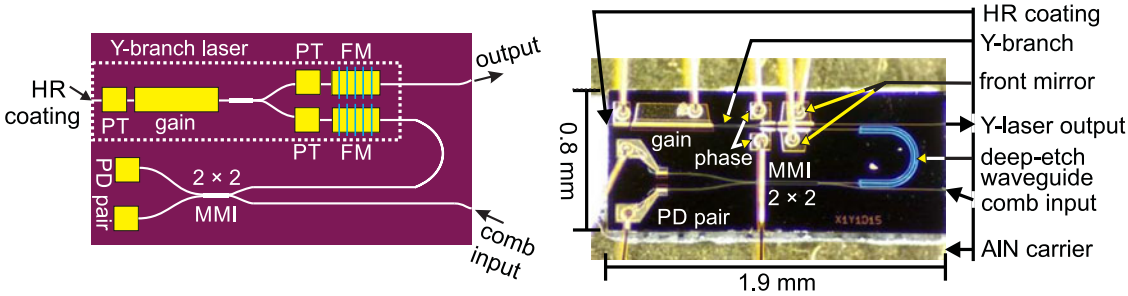

DOI: 10.1109/JPHOT.2017.2696858
1943-0655 © 2017 IEEE

Power-Efficient Kerr Frequency Comb Based Tunable Optical Source

S. Arafin,[1] *Member, IEEE*, A. Simsek,[1] *Student Member, IEEE*, S.-K. Kim,[1] W. Liang,[2] D. Eliyahu,[2] G. Morrison,[3] M. Mashanovitch,[3] *Senior Member, IEEE*, A. Matsko,[2] *Senior Member, IEEE*, L. Johansson,[3] *Member, IEEE*, L. Maleki,[2] *Fellow, IEEE*, M. J. Rodwell,[1] *Fellow, IEEE*, and L. A. Coldren,[1] *Life Fellow, IEEE*

[1]Department of Electrical and Computer Engineering, University of California, Santa Barbara, CA 93106 USA
[2]OEwaves Inc., Pasadena, CA 91107 USA
[3]Freedom Photonics LLC, Goleta, CA 93117 USA

DOI:10.1109/JPHOT.2017.2696858

Manuscript received February 27, 2017; revised April 5, 2017; accepted April 18, 2017. Date of publication April 24, 2017; date of current version May 3, 2017. This work was supported in part by DARPA-MTO under the DODOS project and in part by the National Science Foundation (NSF) under Grant 1402935. A portion of this work was carried out at the UCSB Nanofabrication facility, part of the NSF funded NNIN network. Corresponding author: S. Arafin (e-mail: sarafin@ece.ucsb.edu).

Abstract: We designed and demonstrated a power-efficient highly integrated photonic system, requiring a total power consumption of 1.7 W and producing a spectrally pure coherent optical signal with a wavelength range of 23 nm in the C-band. The system consists of a compact, low-power InP-based photonic integrated coherent receiver, microresonator-based Kerr frequency comb, and agile electronic circuits. The photonic coherent receiver contains a 60-nm widely tunable Y-branch local oscillator (LO) diode laser, a coupler, and a pair of photodetectors. It consumes record-low (approximately 184 mW) electrical power. The optical frequency comb reference has excellent spectral purity, $<$4 kHz optical linewidth, and good frequency stability. The spectrally pure tunable optical source was produced by offset locking the on-chip LO laser of the integrated receiver to this frequency comb source. A possibility of further stabilization of the frequency comb repetition rate by locking to an external radio frequency synthesizer was demonstrated.

Index Terms: Photonic integrated circuits, integrated optics, optical phase-locked loop, heterodyne, optical frequency comb, optical microresonator.

1. Introduction

Over the past couple of decades, numerous research efforts have been devoted to the area of photonic integrated circuits (PICs) [1]–[5]. This is mainly because the cost, size, weight, and combined insertion loss of the on-chip optical components can be significantly reduced through integration, while the stability and performance of the photonic integrated systems can be drastically enhanced. In addition to these obvious advantages, low-power-consumption is also an important motivating factor for photonic integration. The device reliability increases with decreasing power levels, and therefore, PICs contribute to the system reliability to a great extent by reducing its operating electrical power [3]. The associated total thermoelectric cooler (TEC) power consumption also decreases significantly.

Recently, highly integrated optical phase-locked loops (OPLLs) have been found to be one of the most attractive technologies for a number of emerging applications, including optical sensing and frequency synthesis [6]. Many novel compact optical systems in these areas can be developed by using such integrated OPLLs. In this work, we demonstrate the OPLL-based offset locking of an on-chip widely-tunable local oscillator (LO)-laser within the coherent receiver PIC to a microresonator-based optical frequency comb (OFC). This is a major step towards an eventual demonstration of the chip-scale, low-power, ultrastable optical frequency synthesizer. An integrated optical synthesizer is a device that is able to produce a narrow-linewidth optical signal at a desired wavelength. Such a synthesizer can be created by offset locking of a broadly tunable LO laser to an OFC master oscillator (MO).

In addition to the LO and MO, the synthesizer includes a photonic integrated coherent receiver and feedback electronics to realize an OPLL. The photonic receiver receives the mixed output of LO and MO signals and produces an error signal fed into the electronic circuits that tune the phase of the LO in order to match that of the MO. Therefore, high-performance, low-power and compact coherent receiver PICs with an integrated widely-tunable LO are of significant research interest due to their use in optical coherent communication, possibly employing OPLL systems in relatively short links [7].

Researchers have already demonstrated prototype PIC receivers for OPLLs [8], [9]. Very recently, we have shown a highly integrated heterodyne OPLL with an InP-based receiver PIC and commercial-off-the-shelf electronic components [10]. However, the PICs used in these studies consumed 0.5 W of power and their footprint exceeded 2.3 mm^2 [9]–[11]. A significant improvement of these parameters is still needed in designing compact and low-power systems. In this paper, we report on the development of a compact, low-power, coherent receiver PIC and its use in OPLLs for frequency synthesis. Compared to the state-of-the-art results reported in [10]–[12], our photonic receiver circuit is 1.5 times smaller in size, it consumes 2.7 times less electrical power and it exhibits 10 nm wider wavelength tuning. We found that the geometrical size and the electrical power consumption for the PICs can be reduced significantly by careful design. Also, inherent advantages of integration were obtained by making the system much smaller. This is attractive since small PICs enable a short OPLL loop delay which results in a high loop bandwidth.

The coherent receiver PIC in an OPLL system usually consists of a widely-tunable LO laser, optical couplers, and a balanced photodetector pair integrated monolithically. Due to the characteristics of the heterodyne OPLL, the noisy LO laser can be forced to clone the low phase noise of the reference laser within its loop bandwidth. With a good RF offset source, this feature can be maintained while tuning the optical frequency away from the reference with Hz level accuracy. To completely take advantage of the heterodyne OPLL, a spectrally pure OFC source with many stable lines, should serve as the reference. This configuration enables tuning across a wide optical frequency range.

In our experiment, we utilized an OFC oscillator [13] developed specifically for the OPLL. The device involves a high quality factor (Q) crystalline whispering gallery mode resonator (WGMR) heterogeneously integrated on a microphotonic bench with a pump laser. This entire oscillator can be easily integrated on an optical microbench and eventually reproducibly integrated on a PIC [14].

The nonlinear WGMR pumped with continuous-wave (CW) light produces an OFC when the power of the pump exceeds a certain threshold [15]. The process results from an optical phenomenon relying upon both self- and cross-phase modulation in the reonator host material, and it is similar to the modulation instability in optical fiber. The high Q-factor of the WGMR ensures that the pump power required to produce an OFC spanning a few THz does not exceed a few tens of mW. Thus, the low power consumption of the comb reference also contributes to minimizing overall system power. Our OFC spans approximately 23 nm, and it is produced by pumping the WGMR with 20 mW of light at 1550 nm.

Further stabilization of such an integrated OFC using external radio frequency (RF) oscillators is also reported. It was demonstrated previously by means of thermal, thermo-optical, as well as mechanical actuation. However, the microresonator OFC devices were not packaged and the actuation bandwidth was comparably narrow. Here, we use a completely packaged microphotonic

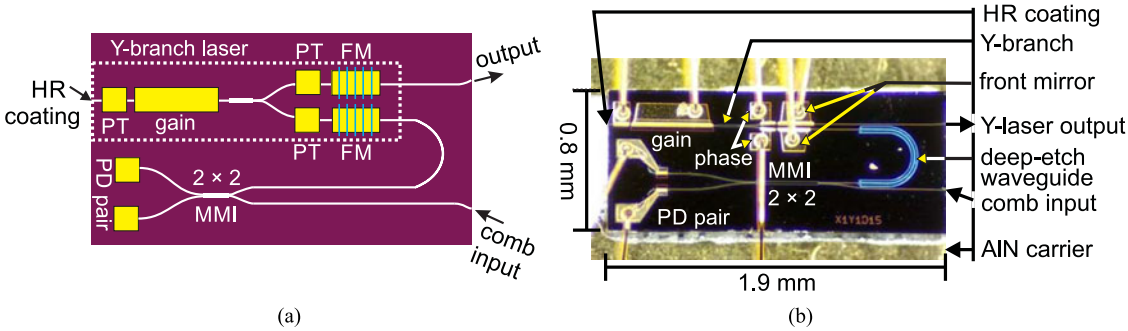

Fig. 1. (a) Functional schematic of the photonic integrated receiver circuit composed of a Y-branch laser, two MMI couplers, and a balanced photodetector pair, as well as (b) microscope image of the PIC mounted on a separate aluminium-nitride (AlN) carrier and wirebonded. (FM: front mirror, HR: high reflection, MMI: multimode interference, PD: photodetector, and PT: phase tuner.)

structure that includes a high-Q WGMR with laminated piezo element (PZT) enabling locking the repetition rate of the OFC to an external source within 100 kHz bandwidth. The demonstrated relative stability of the locking is better than 10^{-14} per hour integration time.

This paper is organized as follows. Section 2 is devoted to a discussion on the newly developed photonic coherent receiver used in this study. The electronic-photonic integration details are described in Section 3. The spectral characteristics of the comb device, as well as heterodyne OPLL results, are presented in Section 4. Operation of the Kerr OFC unit and its stabilization is elucidated in Section 5.

2. Receiver Details

2.1 Design and Fabrication

A widely tunable compact Y-branch laser, a 2 $\times$ 2 multimode interference (MMI) coupler, a balanced photodetector pair and input waveguide are monolithically integrated on an InGaAsP/InP material platform. A schematic of the coherent receiver PIC is shown in Fig. 1(a). The device size is 1.9 mm $\times$ 0.8 mm. For the integration, the offset quantum well (OQW) platform was employed, where the active-region quantum-wells are first grown on top of a common waveguide, and then removed in the regions that are to become passive prior to the regrowth of the top cladding and contact layers. Details of the processing steps for the well-established OQW-based material structure can be found elsewhere [16]. A microscope image of the processed chip is shown in Fig. 1(b), where two output ports after a 1 $\times$ 2 MMI coupler can be seen. For the Y-branch laser design, front grating mirrors on both ports are incorporated. One port is coupled to the integrated coherent receiver, while the second port provides the output signal.

One of the key components in this integrated chip is the Y-branch laser which consumes most of the power. Similar to the sampled-grating distributed Bragg reflector(SG-DBR) laser, the Y-branch laser uses Vernier tuning to reach a wide tuning range. Our design was optimized with a shorter cavity and a highly-reflecting back cleaved/HR-coated mirror for low-power consumption. The high-reflection (HR) coating with a reflectivity of $>$95% at back facet enables a short gain section further shortening the overall length. The front sampled-grating mirrors select wavelength through Vernier tuning but have lower reflection for better efficiency and higher output power. Phase sections are included for continuous tuning. No long absorber section or integrated booster preamplifier was included in this design so that the power consumption and chip-size could be reduced further. The output and input waveguide cleaved facets were coated with antireflection (AR) coating to suppress parasitic reflections.

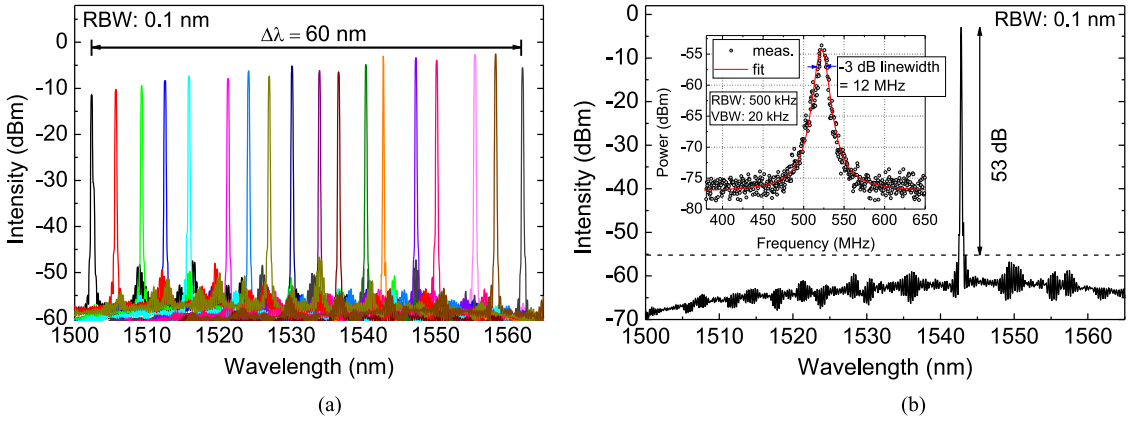

Fig. 2. (a) Superimposed measured lasing spectra of the Y-branch laser with an emission wavelength, ranging from 1502 to 1562 nm, and (b) typical single-mode lasing spectrum at a wavelength of 1543 nm with a side-mode suppression ratio of 53 dB. Beat spectrum of the laser obtained using a heterodyne technique is shown as the inset.

2.2 Spectral Characterization of Y-Branch Lasers

Fig. 2(a) shows the superimposed measured lasing spectra from 1502 nm to 1562 nm. Electrical current in both front mirrors is tweaked to obtain such wide tuning. As can be seen, the tuning range of such a laser is about 60 nm, covering the entire C-band. Any and all wavelengths can be obtained in this range by setting a combination of these mirror currents to set the approximate wavelength window, and then fine tuning of the cavity mode with the phase section, which is controlled by the OPLL in the phase-locked source. Tuning to a particular wavelength is, thus, not done by continuously tuning across the spectrum, but by digitally tuning to the desired wavelength in these two steps. Spurious outputs could be avoided by blanking the output during this process. The peak gain wavelength of the device being tested is blue-shifted. This induces the tuning range of the laser to be shifted towards the shorter wavelength. Fig. 2(b) shows a typical single-mode lasing spectrum of the Y-branch laser at the emission wavelength of 1543 nm. The laser shows good single-mode working performance with a side-mode suppression ratio (SMSR) of 53 dB. SMSRs above 45 dB across the whole tuning range with typical values greater than 48 dB are observed. The linewidths of the Y-branch lasers were also measured, using a heterodyne technique. First, we beat this laser with a narrow linewidth external-cavity laser (ECL) and the beatnote is detected to an external fast photodetector (PD) which converts it into an electrical tone. The RF signal was then measured with an electrical spectrum analyzer (ESA). Thus, before phase-locking, the 3-dB linewidth is measured to be 12 MHz, as shown in the inset of Fig. 2(b).

2.3 Balanced Photodiode Characterization

High bandwidth, low dark current, and high saturation power are the desired characteristics of on-chip photodiodes (PDs). The coherent receiver PIC was characterized by measuring the dark current and bandwidth of the balanced PD pair. The current-voltage (I–V) characteristics at room-temperature are shown in Fig. 3(a) for both PDs. For the quantum-well (QW) PD with the size of $3.3 \times 50\ \mu\text{m}^2$, the dark current is 10 μA at -3 V. The bandwidth of these PDs was measured using a lightwave network analyzer. By sweeping the modulation frequency from the network analyzer, the relative RF response of the photodetectors (PDs) biased at a -3 V was measured. The response, as shown in Fig. 3(b), is normalized at 1 GHz due to the low-frequency noise from the measurement system. In addition to the noise, gain ripples with $\pm$ 3 dB were observed at frequencies below 1 GHz, possibly due to the impedance mismatch between devices under study and the system. The modulation characteristics of these PDs were measured with the device wirebonded. By direct

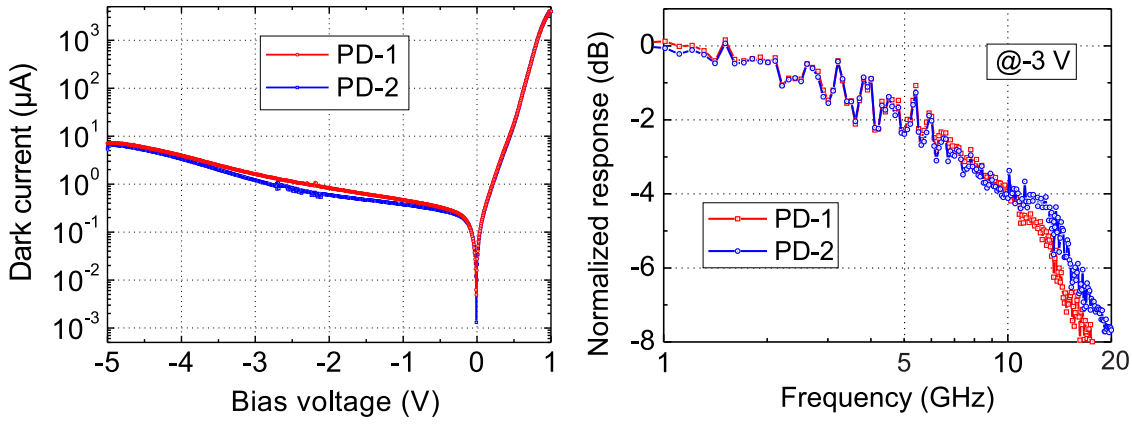

(a) (b)

Fig. 3. (a) Dark currents and (b) modulation characteristics of the two on-chip photodiodes in InP monolithic coherent receiver PIC shown in Fig. 1.

TABLE 1
Total Power Consumption of the Optical Frequency Synthesis System Using Photonic Coherent Receiver Based on Y-Branch Lasers

Element	Section	Number	Current (mA)	Voltage (V)	Power (mW)
PIC	gain	1	73	1.5	109.5
	FM	2	20	1.3	52
	PT	2	7	1.3	18.2
	PD	2	−1	−2	4
EIC	LIA	1	180	3.3	594
	XOR	1	130	3.3	429
	op-amp	1	16	6	96
OFC	pump laser	1	165	2.4	396
	Total		**616**		**1699**

EIC = electronic integrated circuits, FM = front mirror, LIA = limiting amplifier, OFC = optical frequency comb, PD = photodetector, PIC = photonic integrated circuits, and PT = phase tuner. Please note that Erbium-doped fiber amplifier (EDFA) and thermo-electric cooler (TEC) power are not included here.

probing on chip, a better performance is expected. Importantly, the bandwidth of the PDs is large enough that our OPLL system with the sensitive feedback electronic circuits can exhibit the offset locking range as high as 18 GHz [17].

2.4 Power Budget Calculation

Table 1 presents the total maximum power consumption of our photonic coherent receiver based on Y-branch lasers during the full operation, enabling 60 nm wavelength tuning. There are three phase

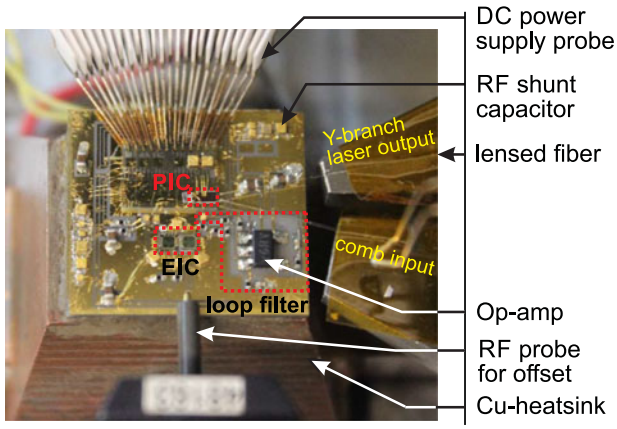

Fig. 4. Microscope image of the entire heterodyne OPLL system where PIC, COTS ICs and loop filter are highly integrated on a separate AlN supercarrier. Finally, it rests on a copper heatsink for the measurement. Two lensed fibers at the right are butt-coupled to the waveguide endface of the photonic chip.

tuning sections integrated in the receiver circuit. The ones, located after the Y-branch and next to the front mirror, are responsible for supermode jumping. In other words, those two phase sections allow us to tune the reflection envelope unlike the one which is located at the far left in Fig. 1. The phase section at the left side of the gain section is responsible for fine emission wavelength tuning, i.e., cavity mode tuning, which was connected to the feedback electronic circuits. It should be noted that it is possible to achieve full wavelength coverage using only two phase sections of the Y-branch laser. One of the phase sections next to the front mirrors can be considered as a redundant. Table 1 also reports the power consumption of other elements, including the packaged OFC unit, EICs, and loop filter components in the overall OPLL.

3. Electronic-Photonic Integration

Fig. 4 shows an image of the heterodyne OPLL system board on the test stage, where PIC, EIC and loop filter (LF) were assembled closely together by wirebonding. This assembly was done by mounting all these three parts on a patterned ceramic supercarrier in close proximity to minimize loop delay. An AC-coupled system was prepared by forming an on-chip bias tee in order to continuously remove DC offsets from the balanced-PD signals. The balanced-PDs reduce the influence of relative intensity noise (RIN) from the LO laser since this noise is common to both detectors.

As a part of the feedback electronics, SiGe-based limiting amplifier (LIA) and logic XOR gate, both manufactured by ADSANTEC [18], were employed. A high-speed emitter coupled logic differential amplifier with a 30 dB differential gain was used as a LIA. It is connected to the balanced PD pair in order to limit and square-up the input PD signals. This helps to make the OPLL system insensitive to PD power fluctuations. This LIA was followed by a high-speed digital XOR gate to obtain the phase difference between the RF beatnote resulting from the beating of the two lasers and a reference signal from a tunable RF synthesizer. Both are commercial-off-the-shelf (COTS) SiGe elements whose details can be found in [18]. A commercial LMH6609 op-amp and discrete surface-mount device (SMD) components were used to build up the LF circuit and its design details are listed in [19]. An additional fast feedforward path was also included in the LF to increase the loop bandwidth to 500 MHz. The output from the XOR gate is smoothed out by the LF to control the LO laser's phase and hence lock the phase of the LO to a single comb line. The OPLL system size is approximately 1.8×1.6 cm^2. The system could be made as compact as 1 cm^2 easily by optimizing the supercarrier design.

4. Offset Locking to Microresonator Comb

4.1 Spectral Characterization of Optical Frequency Combs

An OFC generated using a semiconductor laser pumping a crystalline MgF_2 resonator with a mode spacing of 25.7 GHz was used in this study [15]. The unit was packaged in ~1 inch cubed form factor and its fiber-coupled output was sent to an OSA. The measured optical spectrum with a 50-dB span of 23 nm is shown in Fig. 5(a). The strongest central line at 1555.27 nm originates from residual light of the pump laser. The RF signal generated by beating between comb lines on a fast PD integrated in the packaged unit was measured to distinguish between chaotic and coherent regimes of the frequency comb. An exceptionally high spectrally pure RF line with the coherent comb is observed. The 3-dB beat width of the RF tone at 25.7 GHz is <100 Hz, limited by the resolution bandwidth (RBW) of the ESA [10]. The phase noise of this RF tone is shown in Fig. 5(b). The noise was measured using OEwaves' phase noise test system.

Depending on the initial conditions, the OFC unit produces frequency combs with envelopes varying in shape. The variations can be linked to the generation of a different number of optical pulses within the WGMR. While all the realized coherent states are intrinsically stable and suitable for LO stabilization, the state corresponding to the single pulse localized in the resonator is advantageous as it does not have any envelope structure. Changing of the power of the comb lines makes the offset locking to some of the modes of the OFC a hard task. We tried to utilize the frequency combs with the smoothest envelope.

Fig. 5(b) shows the measured single sideband (SSB) phase noise of the beat of two self-injection locked pump lasers. One of the pump lasers is integrated in our packaged OFC unit. The optical phase noise corresponds to less than 100 Hz instantaneous linewidth of the pump laser is shown in the inset. To determine an effective linewidth, the frequency noise spectrum is derived from the phase noise spectrum by the following relation [20]:

$$S_\nu(f) = 2f^2\mathcal{L}(f) \tag{1}$$

where $\mathcal{L}(f)$ [Hz^{-1}] is the SSB power density of the phase noise, and $S_\nu(f)$ [Hz^2/Hz] the corresponding frequency power noise. The effective instantaneous linewidth $\Delta\nu_{\text{instant}}$ is then given by the minimum of frequency noise multiplied by π [20]

$$\Delta\nu_{\text{instant}} = \pi * \min^{\text{m}}[S_\nu(f)]. \tag{2}$$

To measure the phase noise, two packaged OFC units were used. We tuned them in a way that the combs were produced and then changed the frequencies of the lasers (by changing the frequencies of the resonators) so that the beat note of the lasers did not exceed a few GHz, and measured separately the phase noise of the RF signals produced by the units (by the combs) as well as RF signal produced by the two lasers emitted by the units. Assuming that the lasers are nearly identical, the laser beat phase noise should be reduced by 3 dB with respect to the shown noise to reflect the noise of the single laser. We also studied the spectral purity of the optical comb lines using the heterodyne-technique. The 3 dB linewidth of the RF beatnote created on a fast photodiode by beating a comb frequency harmonic, centered at 1553 nm, and a low noise local oscillator does not exceed 4 kHz, as shown in Fig. 5(c). Measurement with smaller RBW was hindered because of the jitter of the beat note frequency. This clearly suggests that comb lines can be considered as an ultra-narrow linewidth light source.

4.2 Experimental Setup

The comb output from the packaged and fiber-pigtailed OFC unit is optically amplified by an erbium-doped fiber amplifier (EDFA) and finally coupled into the photonic coherent receiver PIC using a tapered lensed fiber. The Y-branch laser output through front mirror was coupled out from the front side of the PIC using a similar lensed fiber for monitoring purposes. An optical isolator was used at the laser output to reduce back reflections. To measure the OPLL tone, the output from the laser was mixed with the comb in an off-chip 2 × 2 coupler, detected via an external high speed

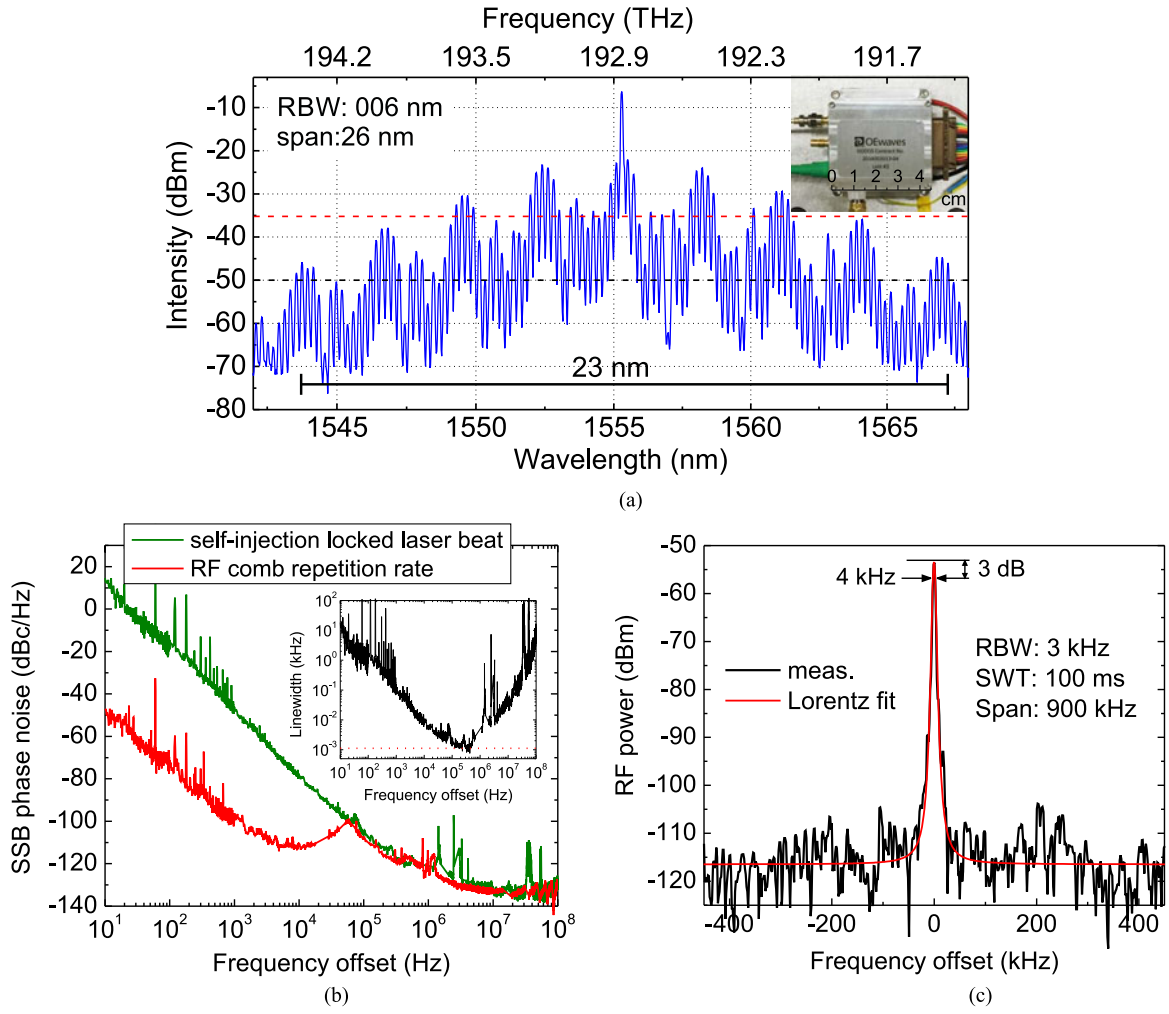

Fig. 5. (a) Optical spectrum of a stabilized Kerr frequency combs generated in the unit, shown in the inset. The comb spans 23 nm, which is defined as the spectral region in which the frequency comb envelope power exceeds −50 dBm (black dotted line) and has a line spacing of 0.2 nm, yielding more than 115 lines. The optical output comb power exiting the fiber obtained after subtracting from the pump laser power is 100 μW, meaning only $\sim$0.5 μW per comb line is accumulated in the wavelength range of 1542 nm-1568 nm. The horizontal (red) dashed line denotes the $\sim$0.5 μW per comb line power level, (b) single sideband (SSB) phase noise of the injection-locked DFB laser, used as a pump laser, integrated in the packaged OFC unit and the RF signal generated by the Kerr comb repetition rate. The instantaneous linewidth of the pump laser is extracted from its phase noise, as shown in the inset. The linewidth of a laser is ill-defined because of flickering and drifting frequency. Various techniques [20], [21] were proposed to circumvent the problem. It is known that frequency noise spectrum is a more relevant entity to characterize the laser performance. To resolve the issue, we utilized the formula $\Delta\nu_{\text{instant}} = \pi * [S_\nu(f)]$, where $S_\nu(f)$ is the corresponding frequency power noise, and $\Delta\nu_{\text{instant}}$ is the effective instantaneous linewidth. Hence, the linewidth is uniquely defined at the particular spectral frequency using the frequency noise values measured experimentally, and (c) RF beatnote, resulting from beating one of the comb lines with ultra-narrow linewidth lasers [22] to measure the optical linewidth of the comb line.

photodetector and measured on the ESA, as shown in Fig. 6. The other output of this coupler was connected to the optical spectrum analyzer (OSA) to measure the optical spectra of Y-branch laser and the comb output. A signal with a frequency equal to the beatnote frequency as a frequency offset was applied from the RF synthesizer to the XOR gate within the EIC.

In order to achieve heterodyne-locking our tunable LO to the comb, the LO wavelength is tuned with respect a comb line to get any random beatnote frequencies, i.e., $\leq$ half of the comb FSR. After

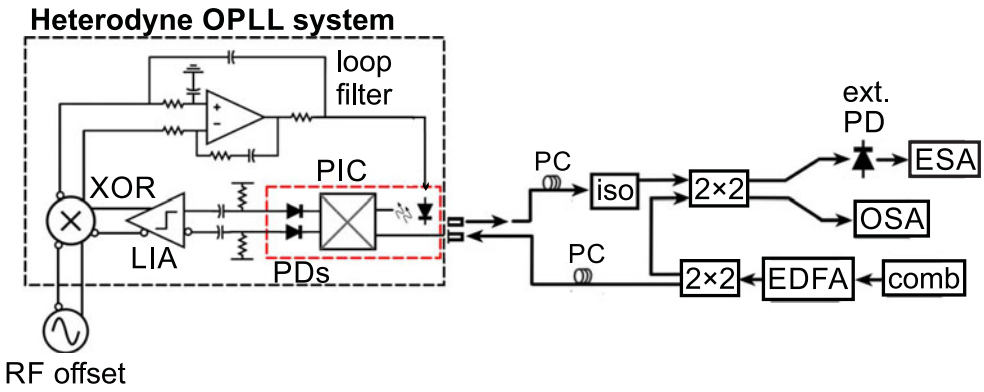

Fig. 6. Test setup of the heterodyne OPLL system for monitoring the performance of the Y-branch laser. (ECL: external cavity laser, EDFA: erbium-doped fiber amplifier, ESA: electrical spectrum analyzer, ext. PD: external photodiode, iso: isolator, LIA: limiting amplifier, OSA: optical spectrum analyzer, PC: polarization controller, and PIC: photonic integrated circuit).

differential PD signals are amplified by the LIA, the RF synthesizer then applies a signal close to the beatnote frequency to the XOR gate. With all feedback electronics is turned on, the XOR gate outputs a signal that becomes zero when the beatnote and RF signal have the same frequency and phase. In other words, the loop filter keeps tuning the LO's phase so that the beatnote signal with a constant offset frequency and phase matches the RF offset. This means that the LO and comb are at a constant phase and frequency offset, i.e., they are phase-locked to each other.

4.3 Locking Results

Our heterodyne OPLL successfully phase locks the Y-branch laser to a comb line up to an offset frequency of 18 GHz with an RF synthesizer. Such maximum offset locking frequency is mainly limited by the operational frequency range of the XOR [18] and on-chip balanced PDs. Since the Y-laser has a tuning range of 60 nm, the whole frequency spectrum within the comb span with a FSR of 25.7 GHz can be utilized for such offset locking. Fig. 7(a) shows the optical spectrum of the Y-branch laser with its emission wavelength 0.046 nm offset from the nearest comb line while the phase locking to this comb line is achieved. This is evidenced by the RF spectrum measured by the ESA at the resolution bandwidth (RBW) of 3 MHz, as shown in Fig. 7(b). The RF beating tones show that the offset frequency is at 5.6 GHz, corresponding to the 0.046 nm. The beat tone generated between the locked Y-laser and the adjacent comb line is also seen at 20.1 GHz. This is expected, since comb lines are stable in phase with respect to each other and the OPLL is phase-locked to the central comb line, hence the OPLL is phase-locked to the adjacent comb line as well. Also, the RF beat tone produced between comb lines is observed at 25.7 GHz, as indicated in Fig. 7(b). Thus, the 23 nm wavelength span of OFC can be covered by tuning the wavelength of our receiver's tunable LO laser. The free running laser has 12 MHz instantaneous linewidth, whereas the relative linewidth of the locked beatnote is less than 100 Hz, revealing excellent relative spectral coherence between the on-chip LO laser and comb. Such a dramatic narrowing of the heterodyne linewidth occurred when the LO laser was phase-locked to the reference OFC. Figs. 7(c)–(e) show the clear coherent peaks of the locked beat note at various RBWs. Sweeping time of each measurement is also shown.

To evaluate the performance of our OPLL system, residual SSB phase noise of the OPLL was measured from 10 Hz to 10 GHz using the setup shown in Fig. 6. The measurement was performed by directly connecting the locked beatnote to a Rohde & Schwarz FSU spectrum analyzer system and using its application firmware (R&S FS-K4). The locked beat note at 3.1 GHz produced between the locked LO laser and the comb was used in this case. The measurement result is shown in Fig. 8. The phase noise variance from 10 Hz to 10 GHz is calculated to be 0.04 rad^2 corresponding to 11.4° standard deviation from the locking point.

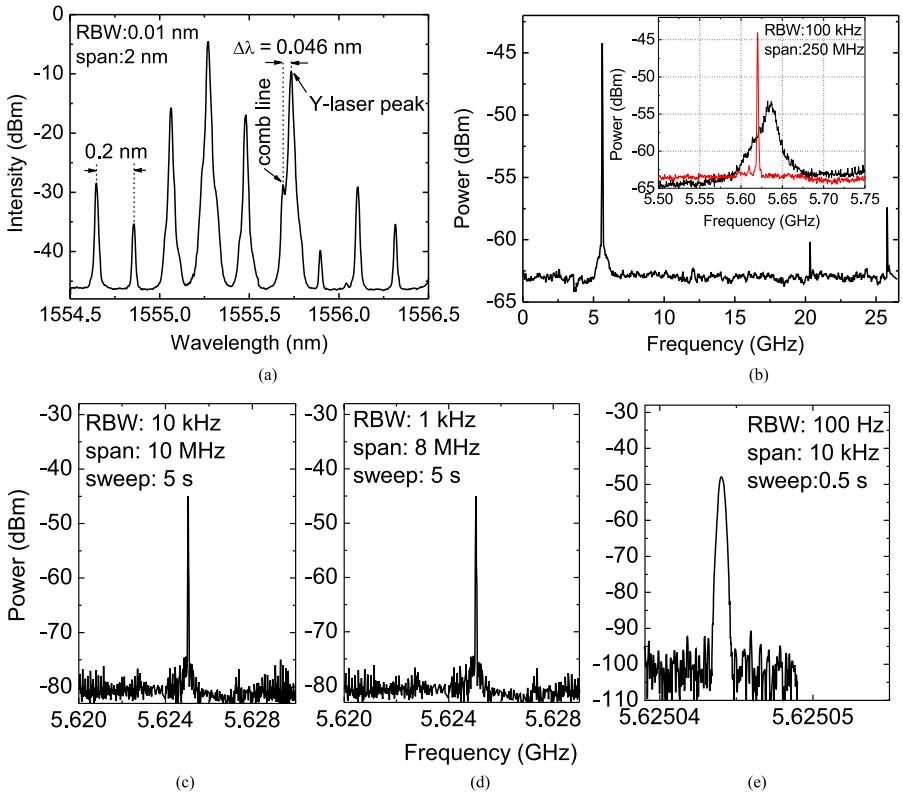

Fig. 7. (a) Optical spectrum when Y-branch laser is offset-locked to the comb at 1555.69 nm with a wavelength difference of 0.046 nm. (b) RF spectrum of the locked beatnote between Y-branch laser and comb at 5.6 GHz is recorded. The beatnote generated between on-chip laser and adjacent comb line at 20.1 GHz and the beatnote produced between comb lines at 25.7 GHz are also visible. The resolution bandwidth is 3 MHz. The zoom-in spectra with a span of 250 MHz is shown as the inset, where the phase-locked (red) and free-running (black) cases can be seen and (c)–(e) measured RF beatnotes at various RBWs.

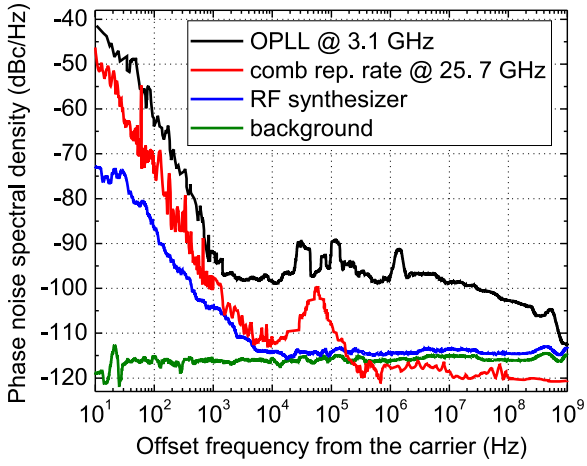

Fig. 8. Single-sideband residual phase noise of the heterodyne OPLL. Phase noise of the RF signal at 25.7 GHz generated by the comb repetition rate, RF synthesizer, and background is also shown here for comparison.

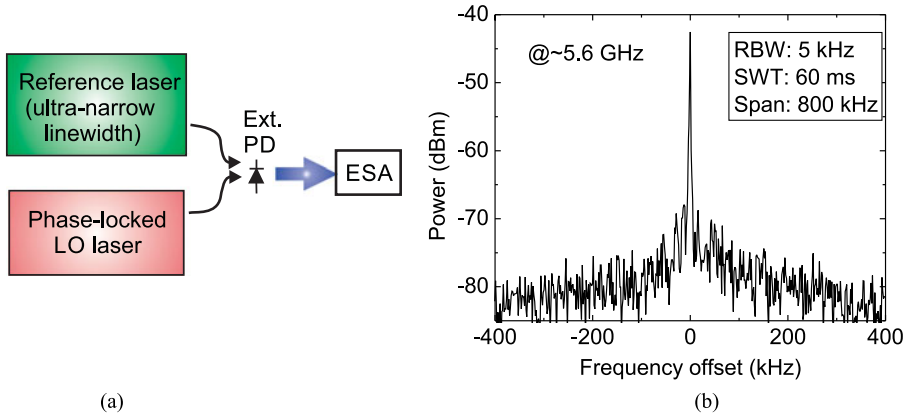

Fig. 9. (a) Out-of-loop measurement setup and (b) optical beatnote resulting from beating the phase-locked LO with other reference ultra-narrow linewidth lasers [22].

In order to measure the linewidth of the locked on-chip laser, an out-of-loop measurement was performed by beating the locked LO with another ultra-narrow linewidth reference laser [22]. Fig. 9 shows the corresponding optical out-of-loop beatnote, showing the linewidth of the laser is approximately the same as the linewidth of the comb harmonic and is $<$5 kHz. Measurement with smaller RBW was hindered because of the jitter of the beat note frequency, as observed earlier. In-loop measurement by mixing the LO laser back with the comb to which we are referencing cannot be used in this regard since a bound phase error which translates in zero frequency error between LO laser and the comb is obtained, once they are phase-locked. In other words, near zero linewidth can then be obtained in the RF spectrum analyzer with the LO offset phase-locked to the comb. Since the LO laser is being forced to instantaneously track the comb line (plus the RF offset) in order to be truly phase locked, common mode noise will not show up in the in-loop beat measurement.

So far, our on-chip tunable lasers are phase-locked to self-referenced and naturally stable OFC lines using heterodyne OPLL. However, further stabilization of OFCs is important for a range of scientific and technological applications, including frequency metrology at high precision, and high-purity optical as well as terahertz frequency synthesis. This stabilization is expected to be a key prerequisite for broadband and low-noise microcomb generation for metrology applications, as well as for integrated micro- and nanophotonic devices. In the next section, we present an effective scheme to achieve a good stability in the OFC, enabling all of these applications.

5. Stabilization of Kerr Frequency Comb

To completely stabilize a coherent mode-locked OFC, one needs to stabilize two of its dissimilar frequencies. Usually, it is desirable to create an octave spanning frequency comb, realize f-2f self-referenced frequency locking, and then either lock the repetition rate or an optical harmonic of the comb to a reference. A single-point locking usually does not reduce frequency drifts of the oscillator significantly. In the case of the Kerr frequency comb oscillator, a single point frequency lock can be instrumental because, unlike conventional mode-locked lasers used for frequency comb production, the microresonator OFC has fewer degrees of freedom: one of its harmonics always coincides with the frequency of the pump light. The pump light is locked to a mode of the WGMR to ensure stable operation of the device. The repetition rate of the frequency comb is partially decoupled from the parameters of the pump light because of the salient properties of the comb oscillator and is impacted mostly by the resonator. Hence, stabilization of the WGMR can stabilize both the pump light and the repetition frequency of the comb oscillator. To achieve the stabilization one needs to actuate the WGMR.

Multiple attempts for stabilization of the Kerr frequency comb oscillator were made [23]–[28]. In some experiments, the comb was locked to a reference femtosecond OFC [23], [24]. The frequency

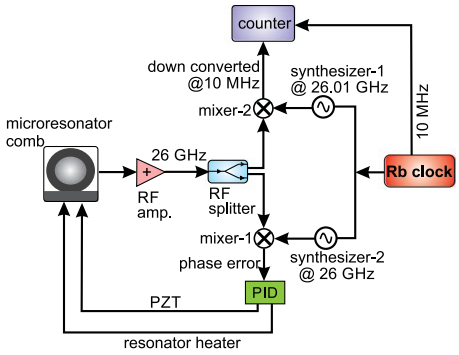

Fig. 10. The experimental setup used for locking Kerr frequency comb to a RF synthesizer. The two RF synthesizers used for phase locking and testing of the OFC are phase locked to a rubidium clock.

and power of the pump light were utilized to achieve the stabilization. Locking the repetition rate of a Kerr comb to a reference RF signal also has been demonstrated [28]. A PZT actuator was used in this case. We here report on stabilizing the repetition rate of the frequency comb using a similar physical principle, but with a heterogeneously integrated OFC.

We created a frequency comb oscillator with a MgF_2 WGM resonator laminated with a PZT actuator. The actuator allows for changing the WGMR radius and stress within the mode localization area. In other words, the frequency of the WGM resonator was altered by changing its temperature as well as by applying stress with a PZT actuator [29]. As a result, the frequency comb repetition rate can be actuated. The actuation bandwidth exceeds 100 kHz.

To lock the repetition rate of the frequency comb to the frequency of an RF synthesizer stabilized to a Rb atomic clock we utilized the PZT actuation. We took a signal from the synthesizer, mixed it with the signal of the comb oscillator and fed it back to the WGM resonator. The locking with PZT worked well, however, the locking range was too narrow with respect to the ambient frequency fluctuations and drifts. The oscillator jumped out of the lock in several minutes after its engagement. We introduced an additional, slow, locking loop utilizing thermal actuation of the resonator. The comb with this approach for stabilization was stable for tens of hours.

The experiment is described by Fig. 10. The 25.7 GHz RF signal coming out of the comb oscillator unit is amplified and split to mix with two synthesizers separately. The frequency of synthesizer #1 is set at 25.71 GHz so the down-converted 10 MHz beat signal can be recorded with a fast counter. The frequency of synthesizer #2 is set to 25.7 GHz. The signal at the output of mixer #2 is processed by a PID controller to lock the RF frequency of the OFC unit through the PZT actuator and a slow actuator (resonator heater). When the frequency difference between the frequency comb oscillator and synthesizer #2 is brought to within the locking range, the feedback loop locked the oscillator to synthesizer #2.

Fig. 11(a) illustrates the measurement of the relative frequency stability of the locked comb frequency measured over 60,000 seconds (blue line) and the calibration measurement (red line). This measurement was performed by Keysight 53152A microwave frequency counter, i.e. not a gapless one. A constant value is subtracted from the data, and therefore, the locked frequency is almost at zero. The comb frequency is locked to a synthesizer according to the previous schematic diagram. In Fig. 11(b), the blue (red) dots show the Allan deviation (AD) of the locked comb (calibration) frequency. For calibration, we measured the AD of the 10 MHz signal created by two RF synthesizers locked to the same Rb clocks.

The absolute stability of the locked comb oscillator is shown in Fig. 12. We locked the comb repetition rate to a Rb clock and compared it to an independent ultrastable quartz oscillator. The data shows that the stability of the locked frequency comb follows the worse of the stability of the clock and the quartz oscillator. Therefore, the developed locking technique allows outstanding locking efficiency for the repetition rate of the OFC. The AD of the self-injection locked pump-laser is also superimposed here. To measure its noise, we used two identical units, beat the lasers on a

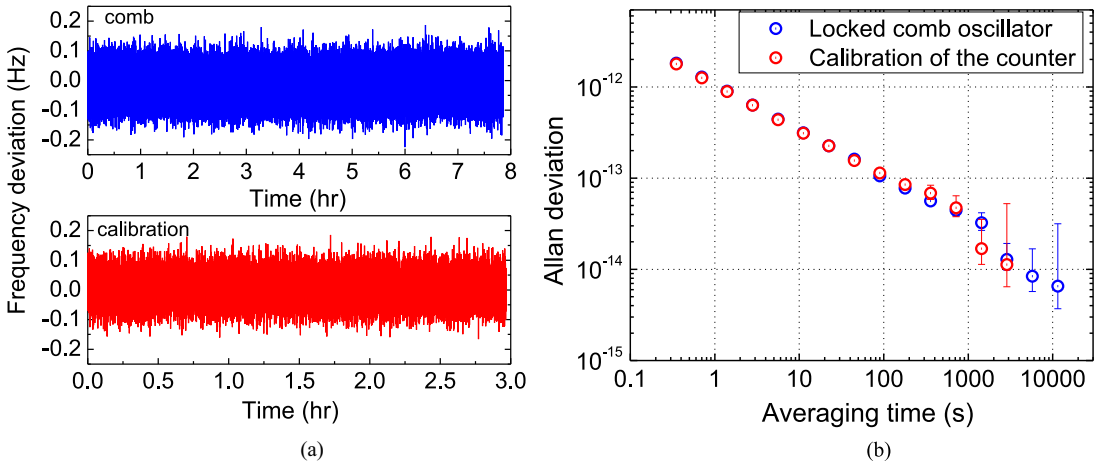

Fig. 11. (a) Relative frequency stability of the locked comb frequency over 60,000 seconds (blue line) and the calibration measurement (red line). A constant value is subtracted from the data so that the locked frequency is almost at zero. (b) Allan deviation measured of the comb frequency after phase locking the comb to a RF synthesizer. As a calibration, the comb was replaced with a synthesizer locked to the same Rb.

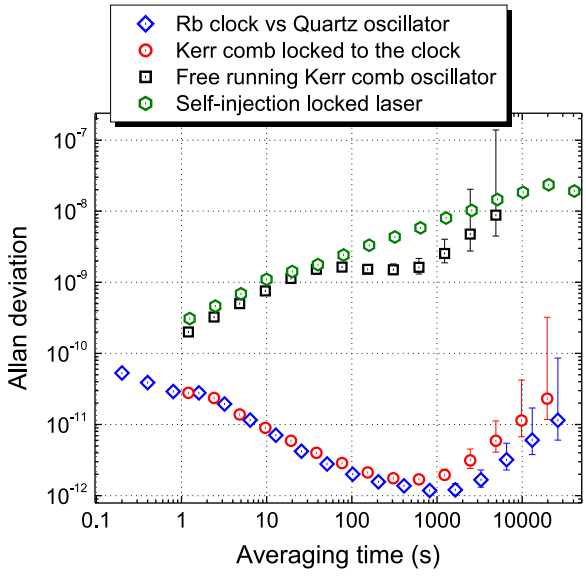

Fig. 12. Absolute stability of the locked Kerr frequency comb after locking the comb repetition rate to the Rb clock. For clarity, the result is compared to an independent ultrastable quartz oscillator. Allan deviation of the self-injection locked pump-laser (not locked to the external RF source) is also superimposed.

PD, measured AD, and then divided the result by $\sqrt{2}$, exhibiting a reasonably good estimation of the laser noise. The AD slighlty increases with integration times.

6. Conclusion

Optical frequency synthesis is realized by means of a highly-integrated heterodyne OPLL with record-low power consumption. Two novel components, including a small and a low power photonic coherent receiver with an integrated broadly tunable laser and an actuatable integrated Kerr frequency comb oscillator are developed and utilized. The demonstrated PIC receiver is promising for reduction of the total power consumption to watt-level in a highly integrated heterodyne OPLL

system, enabling chip-scale optical frequency synthesis across the entire C-band with significant reductions in cost, size, weight, and power. Future work includes designing of the application-specific ICs, consuming only a few hundreds of mW of power. This will enable an OPLL with less than half of a watt of power consumption. An optical frequency synthesizer with a total volume of less than a cubic centimeter and a total power consumption of less than a watt should be possible by interfacing this system with a compact and self-referenced microresonator-based OFC. Such a development is attractive for optical communication, sensing, and imaging.

References

[1] T. L. Koch *et al.*, "GaInAs/GaInAsP multiple-quantum-well integrated heterodyne receiver," *Electron. Lett.*, vol. 25, no. 24, pp. 1621–1623, 1989.
[2] L. A. Coldren *et al.*, "High performance InP-based photonic ICs-A tutorial," *J. Lightw. Technol.*, vol. 29, no. 4, pp. 554–570, Feb. 2011.
[3] D. F. Welch *et al.*, "The realization of large-scale photonic integrated circuits and the associated impact on fiber-optic communication systems," *J. Lightw. Technol.*, vol. 24, no. 12, pp. 4674–4683, Dec. 2006.
[4] J. E. Bowers *et al.*, "Linear coherent receiver based on a broadband and sampling optical phase-locked loop," in *Proc. IEEE Int. Topical Meeting Microw. Photon.*, Victoria, BC, USA, 2007, pp. 225–228.
[5] W. Guo *et al.*, "Two-dimensional optical beam steering with InP-based photonic integrated circuits," *IEEE J. Sel. Topics Quantum Electron.*, vol. 19, no. 4, pp. 6100212(1–12), Aug. 2013.
[6] J. E. Bowers *et al.*, "Chip-scale optical resonator enabled synthesizer (CORES) miniature systems for optical frequency synthesis," in *Proc. IEEE Int. Frequency Control Symp.*, New Orleans, LA, USA, 2016, pp. 1–5.
[7] M. Lu *et al.*, "An integrated 40 Gbit/s optical costas receiver," *J. Lightw. Technol.*, vol. 31, no. 13, pp. 2244–2253, Jul. 2013.
[8] S. Ristic, A. Bhardwaj, M. J. Rodwell, L. A. Coldren, and L. A. Johansson, "An optical phase-locked loop photonic integrated circuit," *J. Lightw. Technol.*, vol. 28, no. 4, pp. 526–538, Feb. 2010.
[9] R. J. Steed *et al.*, "Monolithically integrated heterodyne optical phase-lock loop with RF XOR phase detector," *Opt. Exp.*, vol. 19, no. 21, pp. 20048–20053, 2011.
[10] S. Arafin *et al.*, "Towards chip-scale optical frequency synthesis based on optical heterodyne phase-locked loop," *Opt. Exp.*, vol. 25, no. 2, pp. 681–695, 2017.
[11] M. Lu *et al.*, "Monolithic integration of a high-speed widely tunable optical coherent receiver," *IEEE Photon. Technol. Lett.*, vol. 25, no. 11, pp. 1077–1080, Jun. 2013.
[12] H.-C. Park *et al.*, "40 Gbit/s coherent optical receiver using a Costas loop," *Opt. Exp.*, vol. 20, no. 26, pp. B197–B203, 2012.
[13] W. Liang *et al.*, "High spectral purity Kerr frequency comb radio frequency photonic oscillator," *Nature Commun.*, vol. 6, 2015, Art. no. 7957.
[14] L. Maleki, "Sources: The optoelectronic oscillator," *Nature Photon.*, vol. 5, pp. 728–730, 2011.
[15] A. A. Savchenkov, A. B. Matsko, and L. Maleki, "On frequency combs in monolithic resonators," *Nanophotonics*, vol. 5, no. 2, pp. 363–391, 2016.
[16] J. W. Raring *et al.*, "Advanced integration schemes for high-functionality/high-performance photonic integrated circuits," in *Proc. SPIE*, 2006, vol. 6126, pp. 167–186.
[17] A. Simsek *et al.*, "A chip-scale heterodyne optical phase-locked loop with low-power consumption," in *Proc. Opt. Fiber Commun. Conf.*, Los Angeles, CA, USA, 2017, Paper W4G.3.
[18] [Online]. Available: http://www.adsantec.com/
[19] M. Lu, "Integrated optical phase-locked loops," Ph.D. Dissertation, Dept. Electr. Comput. Eng., Univ. California, Santa Barbara, CA, USA, 2013.
[20] W. Liang, V. S. Ilchenko, A. A. Savchenkov, A. B. Matsko, D. Seidel, and L. Maleki, "Whispering-gallery-mode-resonator-based ultranarrow linewidth external-cavity semiconductor laser," *Opt. Lett.*, vol. 35, no. 16, pp. 2822–2824, 2010.
[21] G. D. Domenico, S. Schilt, and P. Thomann, "Simple approach to the relation between laser frequency noise and laser line shape," *App. Opt.*, vol. 49, no. 25, pp. 4801–4807, 2010.
[22] W. Liang *et al.*, "Ultralow noise miniature external cavity semiconductor laser," *Nature Commun.*, vol. 6, 2015, Art. no. 7371.
[23] P. Del'Haye, O. Arcizet, A. Schliesser, R. Holzwarth, and T. J. Kippenberg, "Full stabilization of a microresonator-based optical frequency comb," *Phys. Rev. Lett.*, vol. 101, no. 5, pp. 053903(1–4), 2008.
[24] P. Del'Haye, S. B. Papp, and S. A. Diddams, "Hybrid electro-optically modulated microcombs," *Phys. Rev. Lett.*, vol. 109, no. 26, pp. 263901(1–5), 2012.
[25] A. A. Savchenkov *et al.*, "Stabilization of a Kerr frequency comb oscillator," *Opt. Lett.*, vol. 38, no. 15, pp. 2636–2639, 2013.
[26] J. D. Jost *et al.*, "All-optical stabilization of a soliton frequency comb in a crystalline microresonator," *Opt. Lett.*, vol. 40, no. 20, pp. 4723–4726, 2015.
[27] J. Lim *et al.*, "Stabilized chip-scale Kerr frequency comb via a high-Q reference photonic microresonator," *Opt. Lett.*, vol. 41, no. 16, pp. 3706–3709, 2016.
[28] S. B. Papp, P. Del'Haye, and S. A. Diddams, "Mechanical control of a microrod-resonator optical frequency comb," *Phys. Rev. X*, vol. 3, no. 3, pp. 031003(1–7), 2013.
[29] W. Liang *et al.*, "Compact stabilized semiconductor laser for frequency metrology," *Appl. Opt.*, vol. 54, no. 11, pp. 3353–3359, 2015.